Cell Reports, Volume *38*

Supplemental information

Endothelial p130cas confers resistance to anti-angiogenesis therapy

Yunfei Wen, Anca Chelariu-Raicu, Sujanitha Umamaheswaran, Alpa M. Nick, Elaine Stur, Pahul Hanjra, Dahai Jiang, Nicholas B. Jennings, Xiuhui Chen, Sara Corvigno, Deanna Glassman, Gabriel Lopez-Berestein, Jinsong Liu, Mien-Chie Hung, and Anil K. Sood

Supplemental Figure 1 Related to Figure 1. Different angiogenic properties of RF24-par and RF24-Bev cells.

(**A**) Bevacizumab (Bev) reduced both total and tyrosine 410-phosphorylated (pY410) p130cas in Bev-sensitive RF24-par cells but not in Bev-resistant RF24-Bev cells. (**B**) Expression of p130cas in RF24-Bev, -par, -Bev-shRNAp130cas, and Bev-shRNA p130cas/WT-p130cas-GFP cells expressing exogenous GFP-tagged WT p130cas. (**C**) Upper: Formation of tube nodes in RF24-par cells, RF24-Bev cells, and RF24-Bev cells with shRNA against p130cas (RF24-Bev-shRNA p130cas). Data are expressed as mean ± SD. *$p < 0.01$(RF24-par versus RF24-Bev; RF24-Bev versus RF24-Bev-shRNA p130cas), two-sided Student *t*-test (n = 3). HPF, high-power field. Representative images for branch sites/nodes formed in each cell type are shown at right. Lower: Cell proliferation represented by the EdU^+ population, which was measured in each type of cells after sorting with FACS. Data are expressed as mean ± SD. *$p < 0.01$, determined by two-sided Student *t*-test (n = 3). (**D**) Resistance to AVA therapy was associated with greater migratory properties of endothelial cells. Left: Representative images of migration of RF24-par or RF24-Bev cells using a modified Boyden transwell chamber coated with gelatin. Right: Graphical comparison of migratory capacities of RF24-par and RF24-Bev cells. Numbers of cells were calculated from 4 random fields per sample. Data are expressed as mean ± SD. *p* value was determined by two-sided Student *t*-test (n = 4). (**E**) Viability of RF24 cells (-par, -par overexpressing p130cas WT, -Bev, and -Bev-shRNA p130cas) treated with VEGF only or VEGF + Bev. Data are expressed as mean ± SD. *$p < 0.05$, determined by two-tailed Student *t*-test (n = 6). (**F**) Viability of RF24-Bev, -Bev-shRNA p130cas, and -Bev-shRNA p130cas/WT p130cas GFP cells treated with VEGF only or VEGF + Bev. Data are presented as mean ± SD. *$p < 0.05$, determined by two-sided Student *t*-test (n = 6). (**G**) Hypoxia decreased p130cas only in RF24-par cells, not in -Bev cells after exposure to 1.0% oxygen (hypoxia [Hypo]) or 20% oxygen (normoxia [Nor]) for 24 hours.

Supplemental Figure 2 Related to Figure 2: Effects of expression and phosphorylation of VEGFR2 in RF24-par and RF24-Bev cells in response to AVA therapy.

(**A**) Mean ΔCt values for mRNA relative expressions of VEGFR2 in RF24-par and RF24-Bev cells by RT-PCR; $p < 0.05$. (**B, C**) Expression or absence of VEGFR2 using CRISPR/Cas9–VEGF Receptor 2 (KDR) Human Gene Knockout Kit (CRISPR, Origene) in RF24-par and -Bev cells. Western blotting with antibodies against VEGFR2 pY1175, pY1214, and total VEGFR2 in RF24-par (B) and -Bev cells (C) stably transfected with scramble control or $VEGFR2^{CRISPR/Cas9\ KO}$. We used β-actin as loading control. (**D, E**) Representative plots of $SYTOX^+$ populations from FACS analysis of RF24-par $VEGFR2^{CRISPR/Cas9\ KO}$ (D) or RF24-Bev $VEGFR2^{CRISPR/Cas9\ KO}$ (E) cells treated with control (CTL), VEGF only, or VEGF + Bev. n = 3; data are expressed as mean ± SD, ns, not significant; two-tailed Student *t*-test. (**F, G**) RF24-par and -Bev cells were pretreated with 0.01 μM pazopanib for 3-4 hours followed by VEGF-A stimulation (10 ng/mL) or VEGF-A (10 ng/mL) + Bev (5μg/μl) treatment. Representative plots of $SYTOX^+$ populations from FACS analysis of RF24-par (F) and-Bev cells (G), n = 3, $p < 0.001$, or ns = not significant; two-tailed Student *t*-test. (**H, I**) Expression of VEGFR2 pY1175, pY1214, and total VEGFR2, as well as pY410-p130cas and total p130cas, was determined by western blotting from protein lysates of RF24-par and -Bev cells pretreated

with 0.01 μM pazopanib and followed by VEGF-A stimulation (10 ng/mL) or VEGF-A (10 ng/mL) + Bev (5 μg/μl) treatment. The ~100-kD fragment of VEGFR2 and 35-kDa fragment of p130cas were observed in RF24-par cells under the VEGF + Bev treatment. We used β-actin as a loading control for both.

Supplemental Figure 3 Related to Figure 2: Caspase-10 is crucial for the cleavage and production of nuclear VEGFR2 in endothelial cells.

(A) ExPASy protein sequence of human VEGFR2 (NP_002244.1) from aa 841-900 showing a unique single caspase-10 (as shown in blue) cleavage site at 852 aa. **(B)** Selection of human caspase-10 (casp10)-CRISPR/Cas9-KO clones in RF24-par endothelial cells. **(C)** In comparison with RF24-par WT cells (left), knockout of caspase-10 with CRISPR/Cas9 (right) diminished the distribution of 100-kD VEGFR2 fragments in the nuclear fraction (NER) under the VEGF + Bev treatment. Other fractions, including cytoplasmic fraction (Cyto) and membrane fraction (MEB), all had expression of VEGFR2 fragments.

Supplemental Figure 4 Related to Figure 2: **AVA therapy drives VEGFR2 and p130cas internalization into LC3B loci in autophagosomes and nuclei in endothelial cells. (A)** Single-channel, high-resolution confocal images of RF24-par cells with immunofluorescence staining with Hoechst (blue)/LC3B (green)/VEGFR2 (red) or **(B)** Hoechst (blue)/LC3B (green)/p130cas (red). Scale bar = 50 μm. Each experiment was repeated at least 3 times, and representative images from 15 high-power fields in each condition are shown. The segmentation algorithm involved detection of nuclei using the Hoechst channel and cell body detection using the red channel (VEGFR2 or p130cas) with adjacent cell splitting based on 1 nucleus per cell and cell body signal intensity. For each cell, the sum of the red channel intensity in the cytoplasm and nucleus was exported to Excel to then calculate the nucleus-to-whole cell intensity ratios. Statistical analysis and graphing was performed in GraphPad Prism. $p < 0.001$ or $p < 0.01$; data are expressed as mean ± SD, two-tailed Student *t*-test.

Supplemental Figure 5 Related to Figure 2: Nuclear distribution of VEGFR2 in RF24 cells in response to AVA therapy. **(A)** Representative Vectra images of RF24-par cells staining with Hoechst (blue)/VE-cadherin (green)/VEGFR2 (red) under control (CTL), VEGF, and VEGF + Bev treatments. Each experiment was repeated at least 3 times, and representative images from 15 high-power fields in each condition are shown. Scale bar = 50 μm. (B) The segmentation algorithm involved nuclear VEGFR2 detection using red and Hoechst channels and cell body detection using the green channel (VE-cadherin). For each cell, the sum of the red channel intensity in the nucleus was exported to Excel to calculate the cytoplasm-to-whole cell intensity ratios. Statistical analysis and graphing were performed in GraphPad Prism software. $p = 0.004$, ns = non-significant; data are expressed as mean ± SD, two-tailed Student *t*-test.

Supplemental Figure 6 Related to Figure 3: Distribution of ~100-kD VEGFR2 fragments in the nucleus occurred only in endothelial cells, not in epithelial tumor cells.

(A) RF24-par cells were treated with VEGF + bevacizumab (Bev) for 24 hours followed by incubation for 48 hours in full medium without Bev, or were continuously treated with VEGF + bevacizumab (Bev) for 72 hours. After subcellular fractionation, fractions were subjected to immunoblotting with anti-VEGFR2 and anti-lamin B1 (LMNB1). (B) Subcellular fractions from human G1S1 dermal endothelial cells and mouse ovarian endothelial cells (MOECs) which had been treated with VEGF + AVA (Bev: 5 μg/mL for G1S1 or B20 4.1.1: 50 ng/mL for MOECs [1]) were subjected to immunoblotting with anti-VEGFR2 (cytoplasmic fraction [Cyto]) and anti-LMNB1 antibodies. The 100-kD fragments of VEGFR2 were observed in nuclear (NER) fractions of both endothelial cell types. (C) SKOV3 ovarian cancer cells treated with VEGF only or VEGF+ Bev were subjected to subcellular fractionation and immunoblotting with anti-VEGFR2 (cytoplasmic portion), anti-LMNB1, and anti–β-actin antibodies. In all experiments, LMNB1 was applied as nuclear fraction control and β -actin as cytoplasmic fraction control**.**

Supplemental Figure 7 Related to Figure 4: TNKS1BP1 chaperones nuclear VEGFR2 fragments as a death factor in response to AVA therapy in RF24-par endothelial cells. (A) RF24-par cells overexpressing Myc-human VEGFR2 (ORF)-DDK were treated with VEGF + Bev and subjected to subcellular fractionation. The nuclear fractions (NERs) were probed with an anti-Flag DDK antibody. (B) Identification of the proteins associated with nuclear VEGFR2 fragments as detected by liquid chromatography-tandem mass spectrometry. The factors listed were the most frequently occurring in immunoprecipitates pulled down by the anti-Flag antibody from the NER fractions of RF-24 cells treated with VEGF + Bev. (C) Transient knockdown of TNKS1BP1 by esiRNA reduced the sensitivity of endothelial cells to AVA therapy. Two esiRNA human TNKS1BP1 complexes and a scramble siRNA were applied to knock down TNKS1BP1 in RF24-par cells. β–actin was used as loading control. (D) Graphical representation of $SYTOX^+$ populations as the percentage of dead cells for each treatment group, including control, scramble siRNA, and esiRNA1 against TNKS1BP1. Figure are expressed as mean ± SD (p = 0.003 for VEGF only versus VEGF + Bev in scramble siRNA cells; $p > 0.05$ (ns=non-significant) for VEGF only versus VEGF + Bev in esiRNA1-TNKS1BP1 cells). The significance of differences between groups was determined by two-tailed Student *t*-test (n = 3); ns, not significant.

Supplemental Figure 8 Related to Figure 4: Effects of knockdown of TNKS1BP1 in RF24-Bev cells in response to Bev treatment. (A, B) Representative FACS plot shows increased $SYTOX^+$ population (A) and formation of acidic vesicular organelles, detected by acridine orange staining (B) in RF24-Bev cells stably expressing TNKS1BP1-shRNA and treated with VEGF + Bev. Error bars represent standard deviations; unpaired two-tailed *t*-test, (A& B). ns = non-significant,

Supplemental Figure 9 Related to Figure 5: Silencing host p130cas using CH-NP-RGD murine-specific siRNAs increases autophagy, nuclear VEGFR2, and cell death in tumor-associated endothelial vasculature. (A) Species specificity of murine-p130cas siRNAs. Immunoblot analysis of p130cas protein expression following *in vitro* transfection with human-specific (siRNA-hs130cas) or murine-specific (siRNA-mp130cas) p130cas siRNAs at 48 hours in mouse ovarian endothelial cells (MOECs) and human ovarian cancer (SKOV3) cells. β-actin was used as a loading control. (B) Left: Representative images of dual immunofluorescent staining of LC3B (green) and mouse CD31 (red) in OVCA432 tumors from mice treated with CH-NP-RGD-control siRNA or RGD-CH-NP-siRNA against murine-specific p130cas (n = 3). Hoechst staining (blue) was used to indicate nuclei. Right, upper: Microvessel density (MVD) was calculated by averaging MVDs from three random high-power fields (HPF) per sample (p = 0.003, n = 3). Right, lower: Numbers of $LC3B^+$ and $CD31^+$ endothelial cells were calculated from the same sets of images ($p < 0.05$). (C) Left: Representative images of staining of p130cas (green) and mouse CD31 (red). Right: Numbers of $p130cas^+$ and $CD31^+$ endothelial cells were calculated by averaging from four random HPFs per sample (p <0.001, n = 4). (D) Representative images of staining of VEGFR2 (green) and mouse CD31 (red) (n = 4). (E) Left: Representative images of staining of TUNEL (green) and mouse CD31 (red). Right: Numbers of $TUNEL^+$ and $CD31^+$ endothelial cells were determined by averaging from four random HPFs per sample (p <0.001). Figure are expressed as mean ± SD, determined by two-sided Student *t*-test (n = 4). Scale bar = 100 μm.

Supplemental Figure 10 Related to Figure 5: Genomic ablation of vascular p130cas inhibits tumor progression and prolongs survival in syngeneic models with adaptive resistance to AVA therapy. (A) Kaplan-Meier survival plot of C57/BL6 WT, $p130cas^{flox/flox}Tie2^{CRE}$, Tie2cre, and $p130cas^{flox/flox}$ mice bearing intraovarian ID8 tumors and receiving either control IgG antibody or anti-VEGF antibody (B20) treatments. (B) Representative gross images from mice from each group with C57/BL6 background and carrying syngeneic ID8 tumors, which were implanted surgically into the left ovary of each mouse. Progression of ID8-luciferase tumor burden demonstrated with bioluminescence in each group. (Photon emission was measured in each mouse, and means are shown.)

Supplemental Figure 11 Related to Figure 5: Silencing vascular p130cas in $p130cas^{flox/flox}Tie2^{Cre}$ mice increased endothelial cell autophagy as well as nuclear distribution of p130cas/VEGFR2/TNKS1BP1 in syngeneic ID8 tumor tissues. (A) Left: Representative images of staining of mouse CD31 (green) and p130cas (red). Right: Numbers of $p130cas^+$ and $CD31^+$ endothelial cells were averaged from four random high-power fields (HPFs) per sample (p <0.001). Data are expressed as mean ± SD, determined by two-sided Student *t*-test (n = 4). (B) Left: Representative images of dual immunofluorescence staining of mouse CD31 (green) and LC3B (red) in ID8 tumors implanted in the left ovaries of mice, which were then treated with B20. Right, upper: Microvessel density (MVD) was calculated by averaging MVD from four random HPFs per sample (p <0.001). Right, lower: Numbers of $LC3B^+$ and $CD31^+$ endothelial cells were calculated from the same set of images (p = 0.03). Hoechst staining (blue)

indicates nuclei. (C) Representative images of staining of mouse CD31 (green) and TNKS1BP1 (red). TNKS1BP1 was elevated in the ID8 tumors from p130cas$^{flox/flox}$Tie2^{Cre} mice. (D) Representative images of staining of mouse CD31 (green) and VEGFR2 (red). The distribution of VEGFR2 in the ID8 tumors from C57/BL6^{WT} (low VEGFR2 in CD31^{+} cells) was distinct from that in p130cas$^{flox/flox}$Tie2^{Cre} mice (high VEGFR2 in CD31^{+} cells). Scale bar = 100 μm.

Supplemental Figure 1

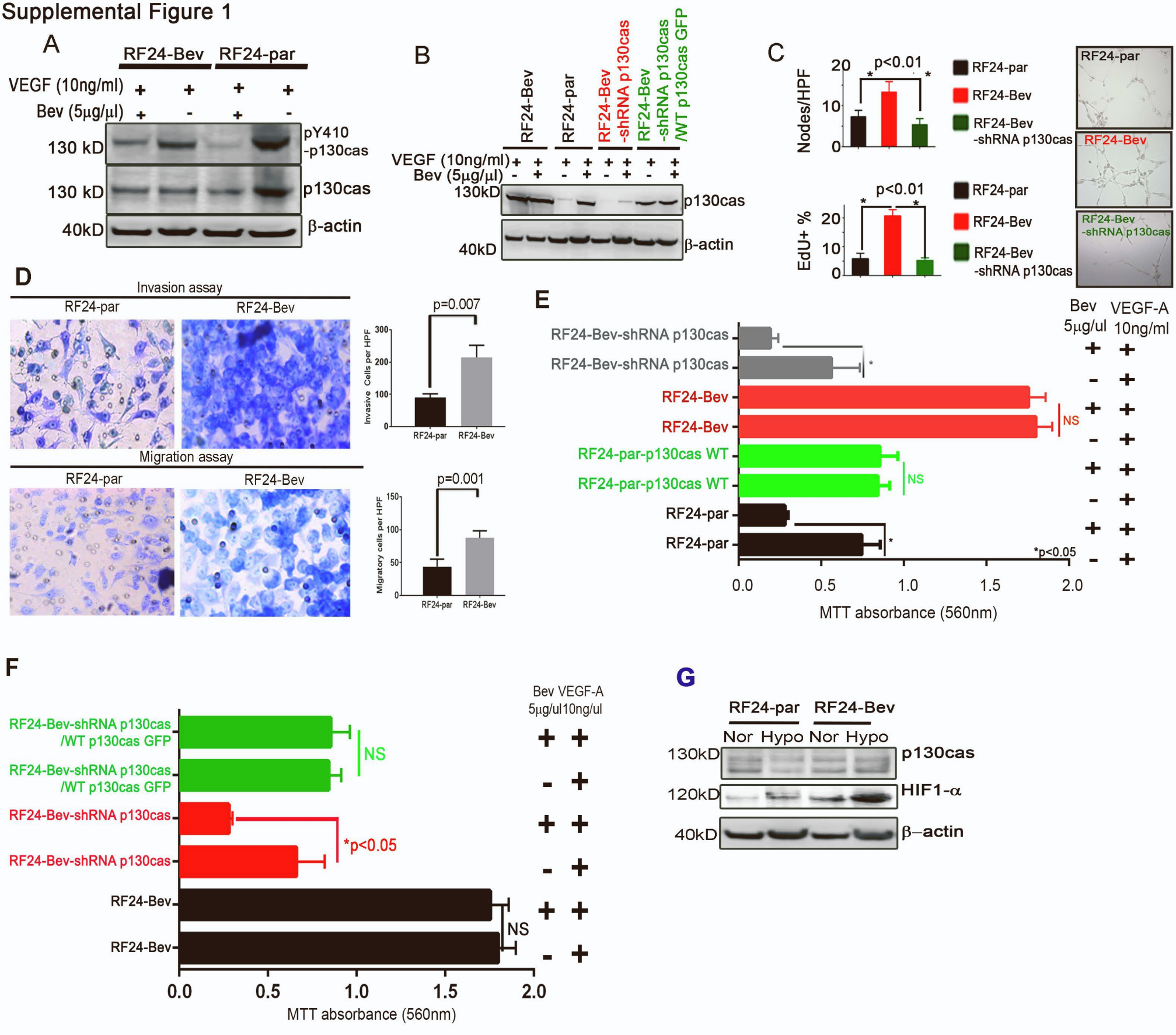

Supplemental Figure 2

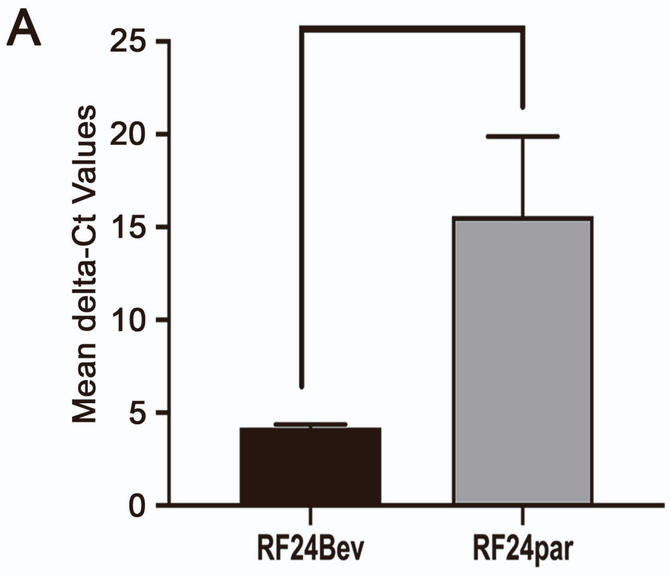

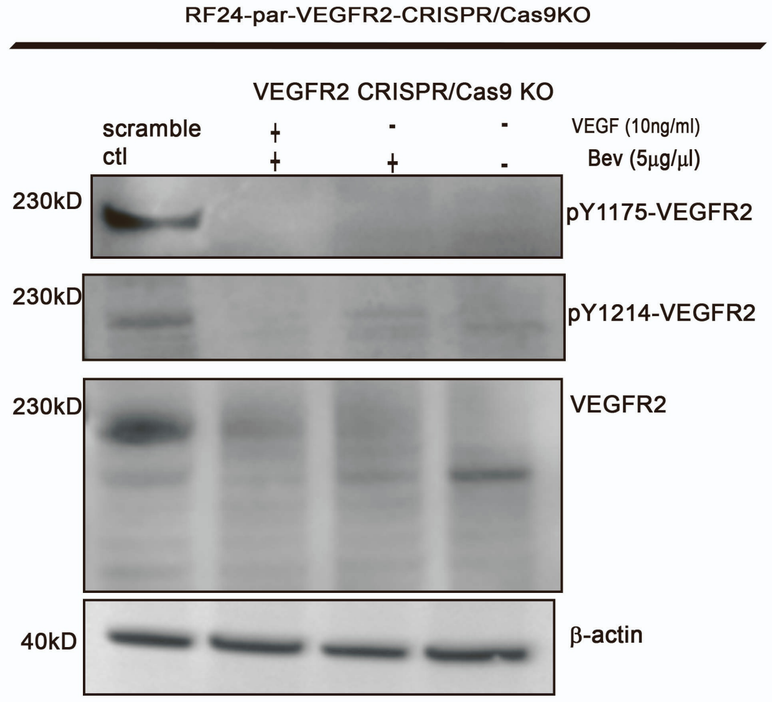

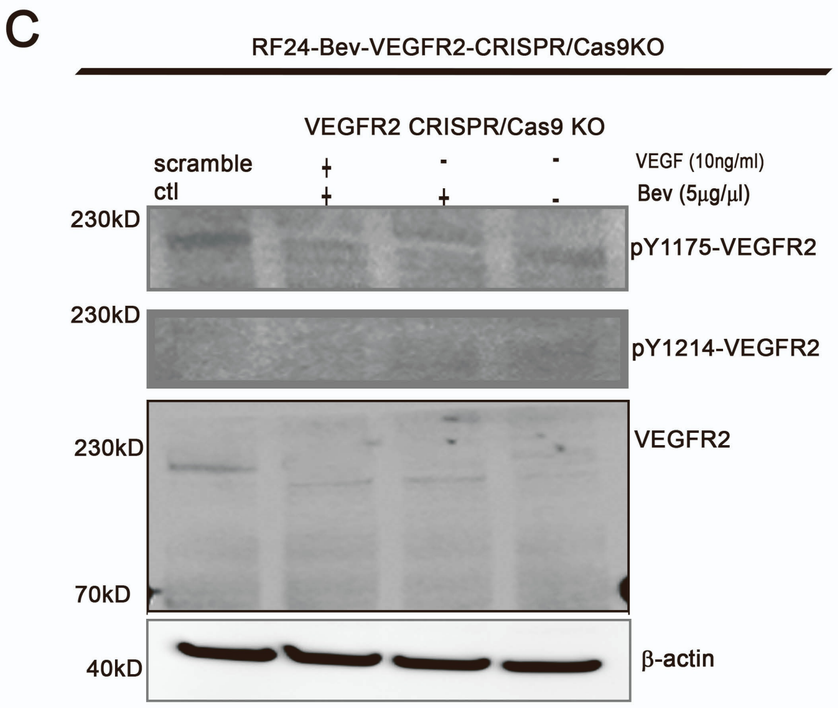

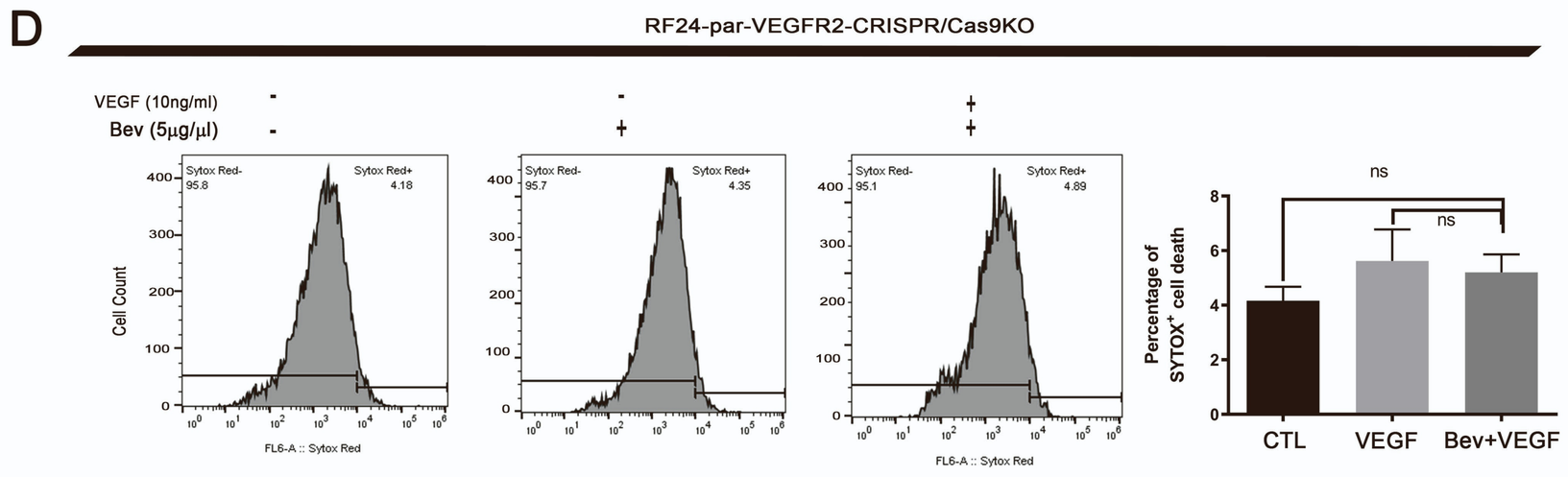

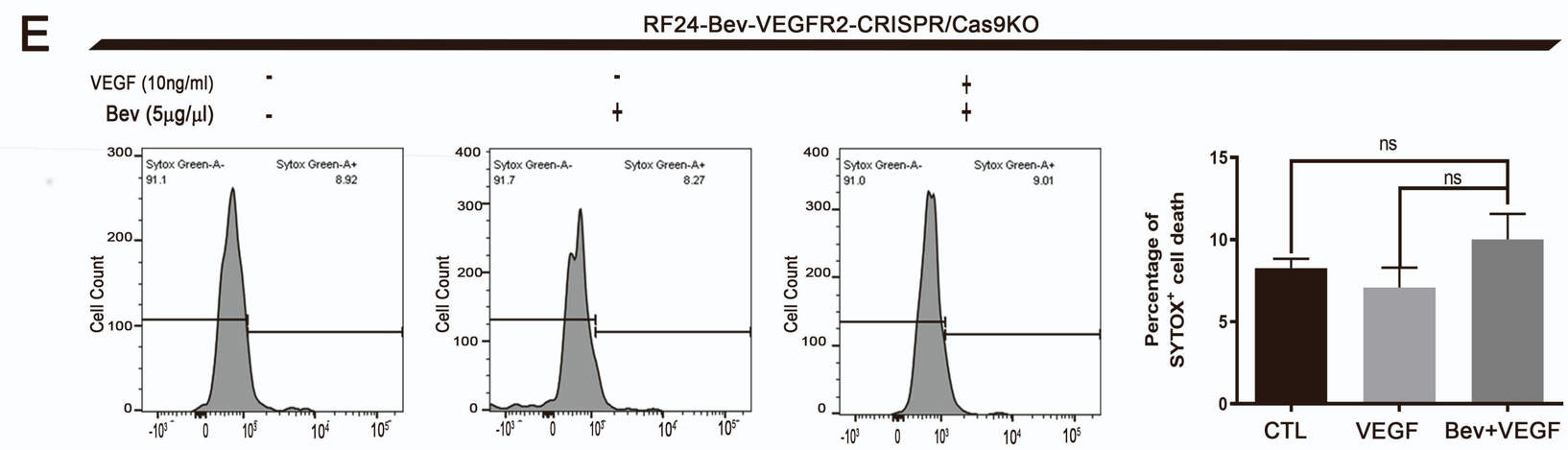

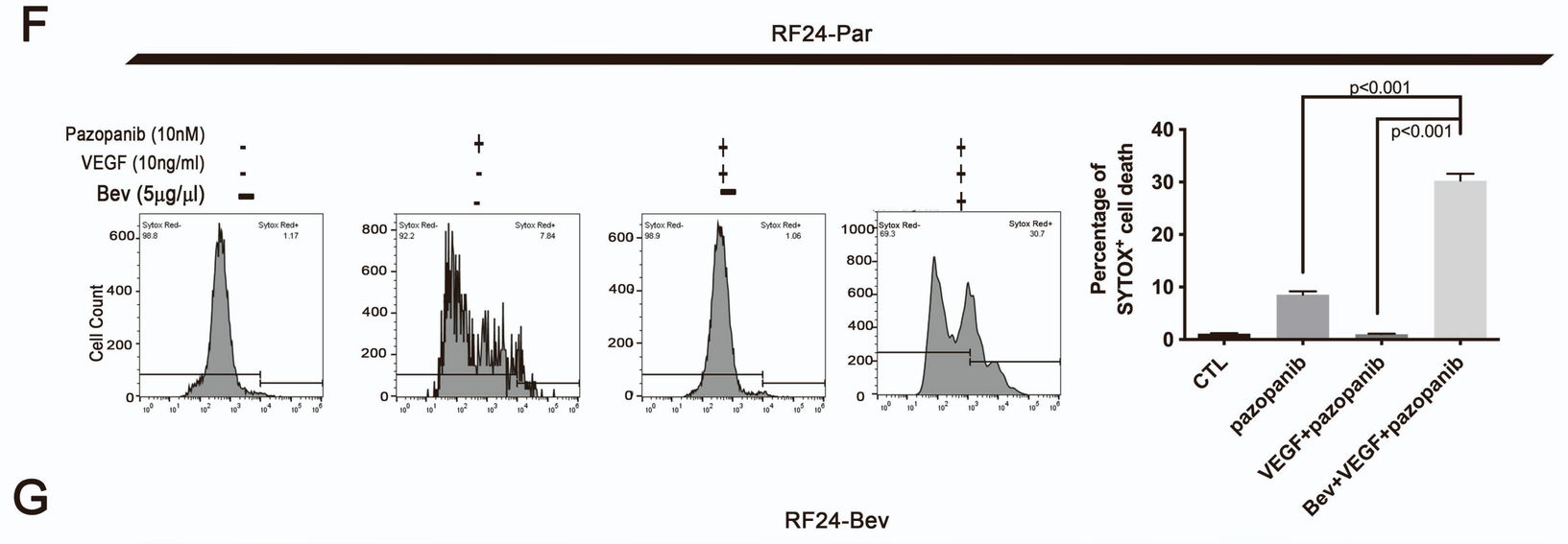

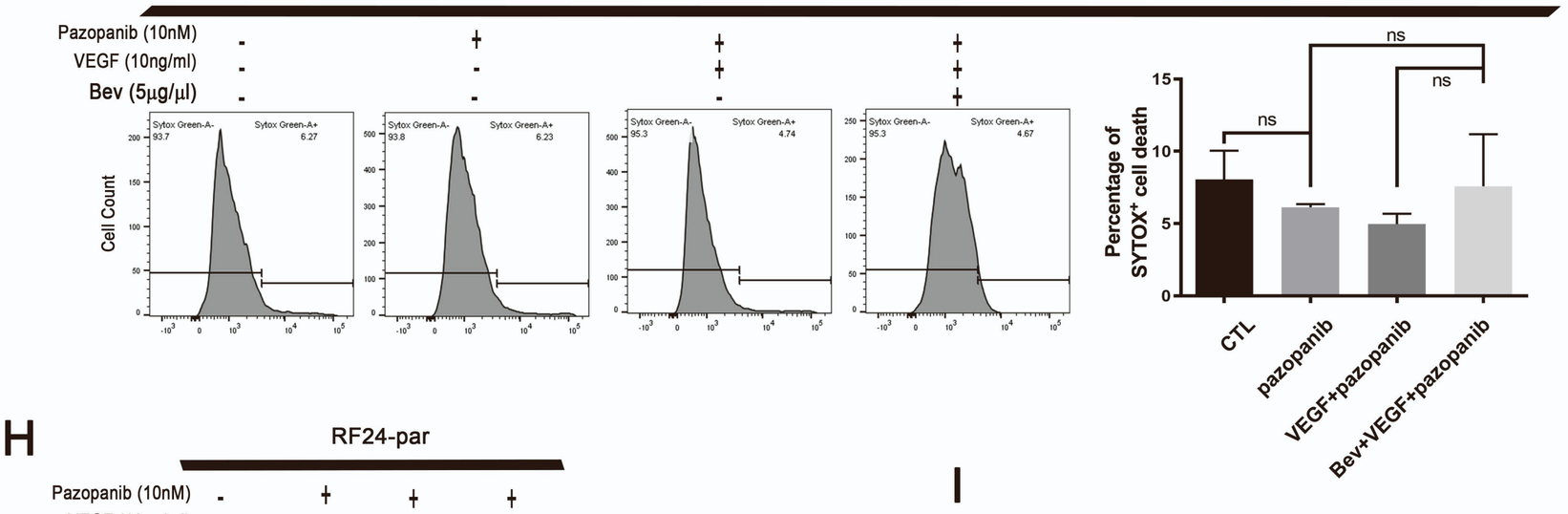

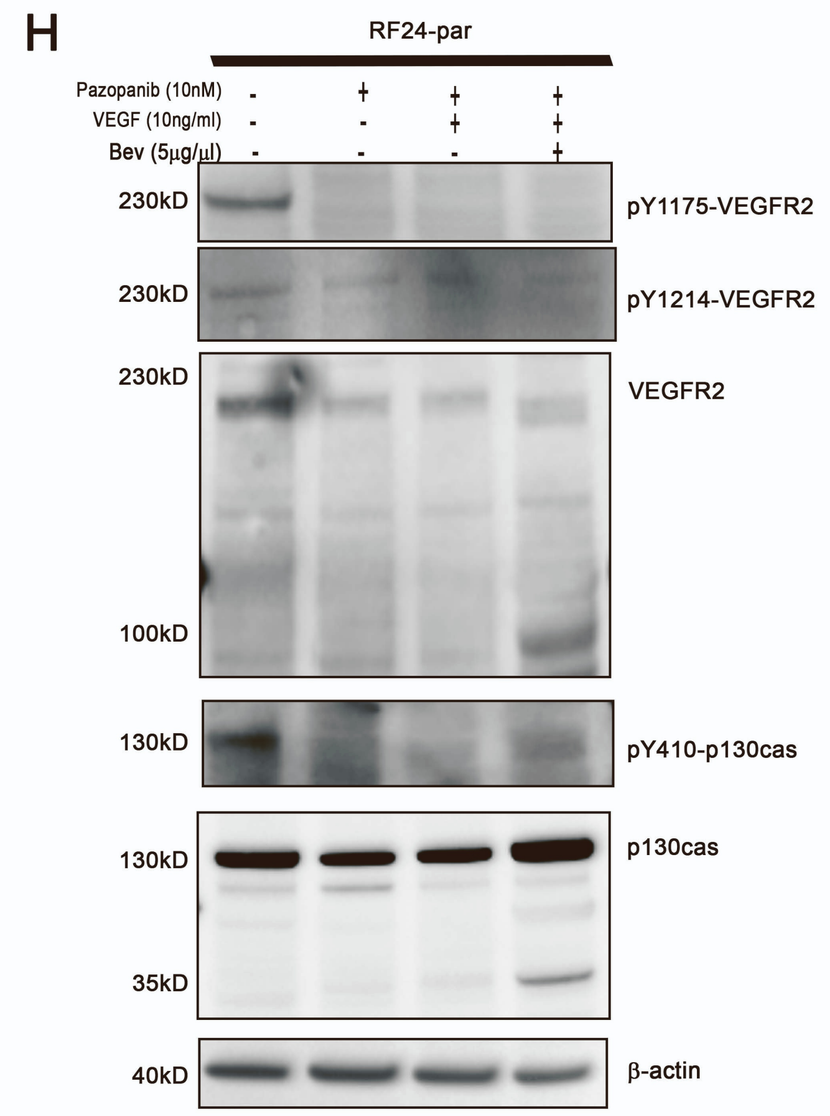

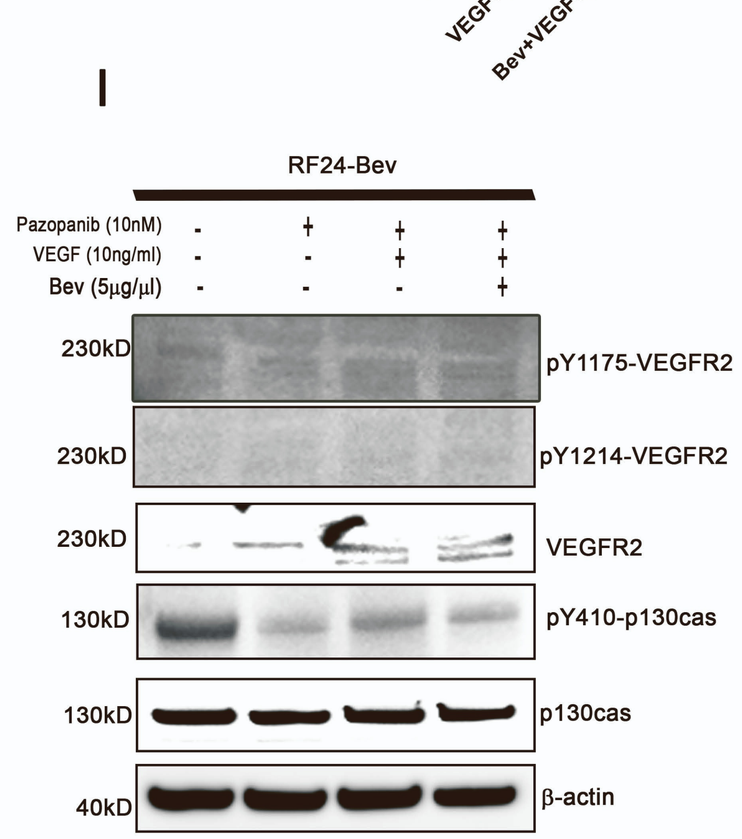

Supplemental Figure 3

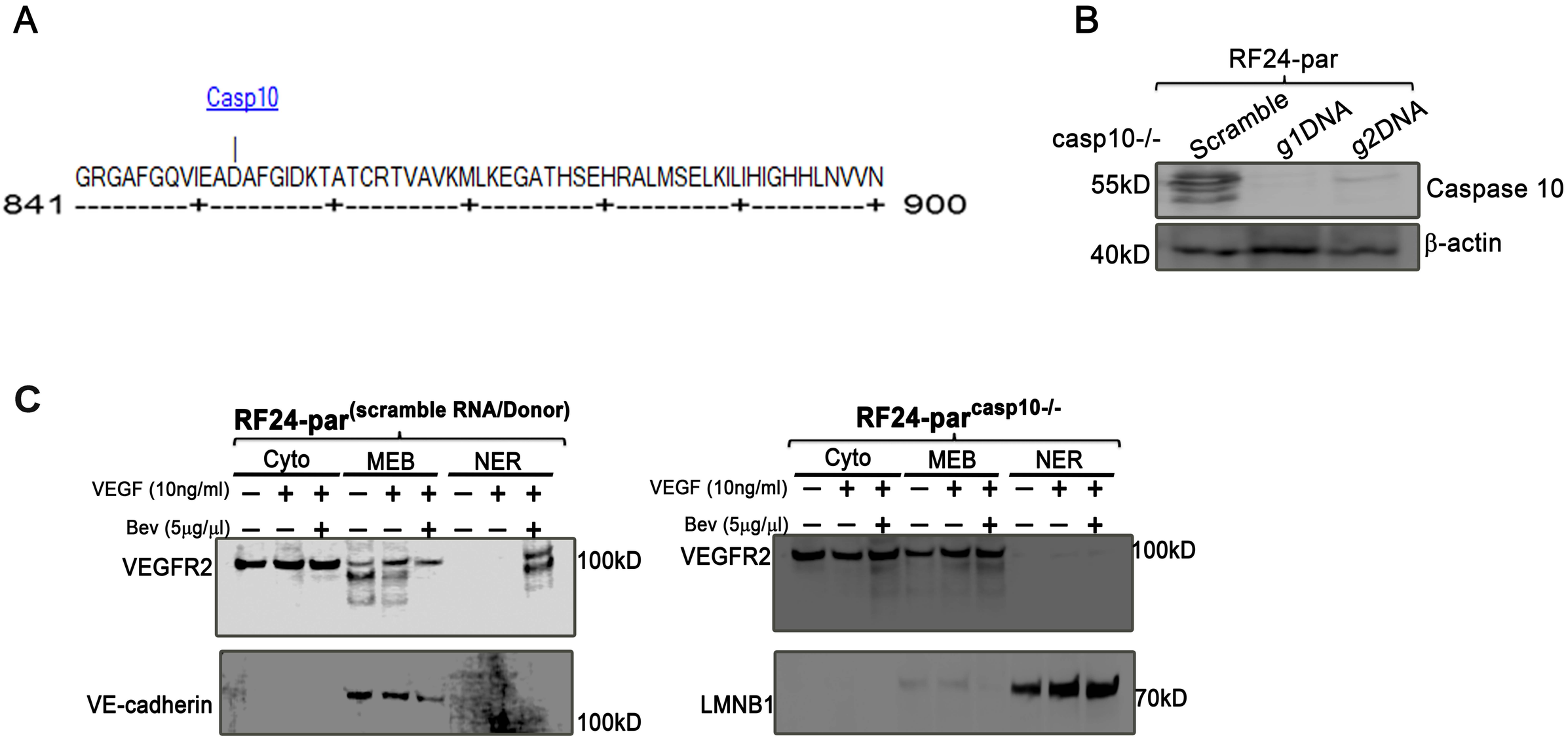

Supplemental Figure 4

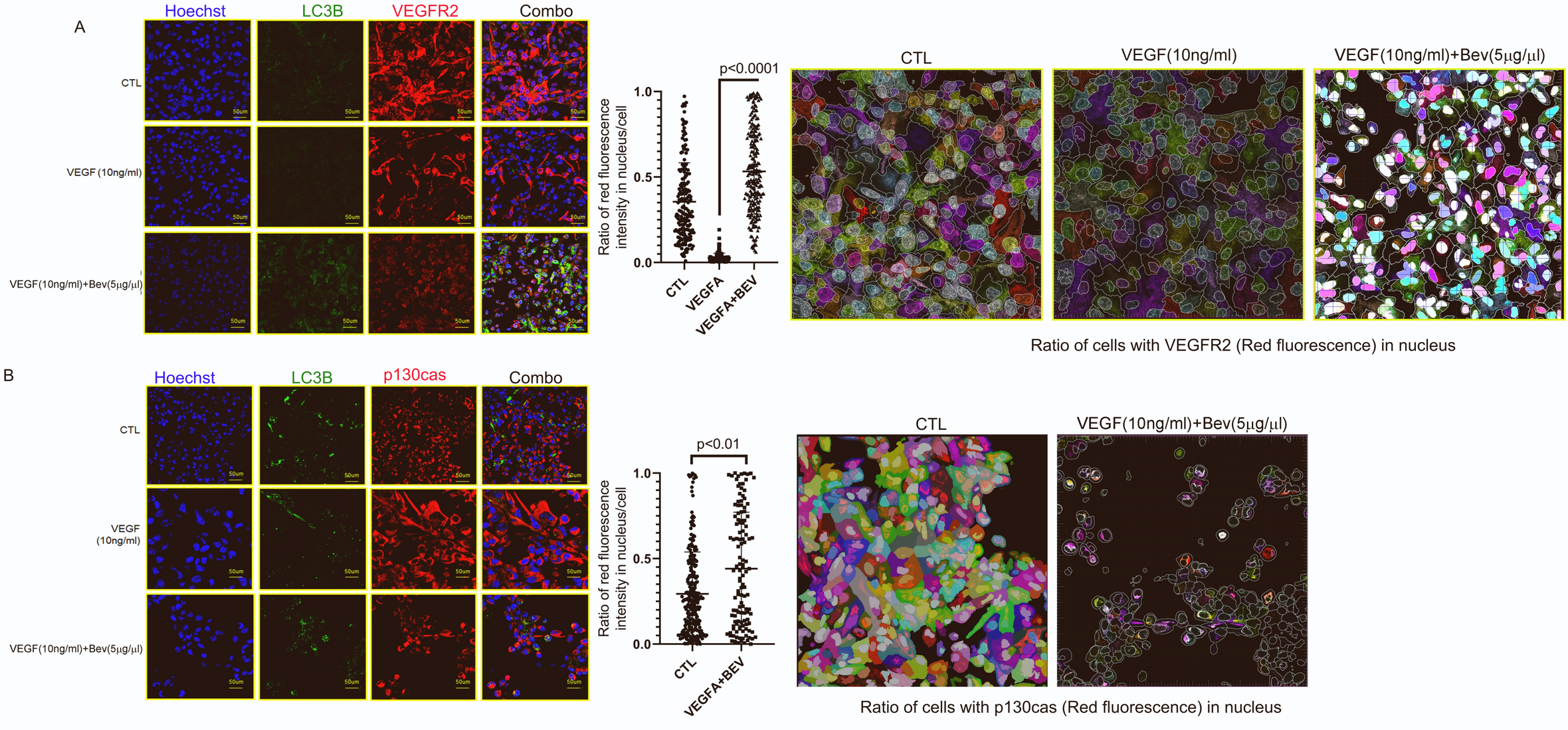

Supplemental Figure 5

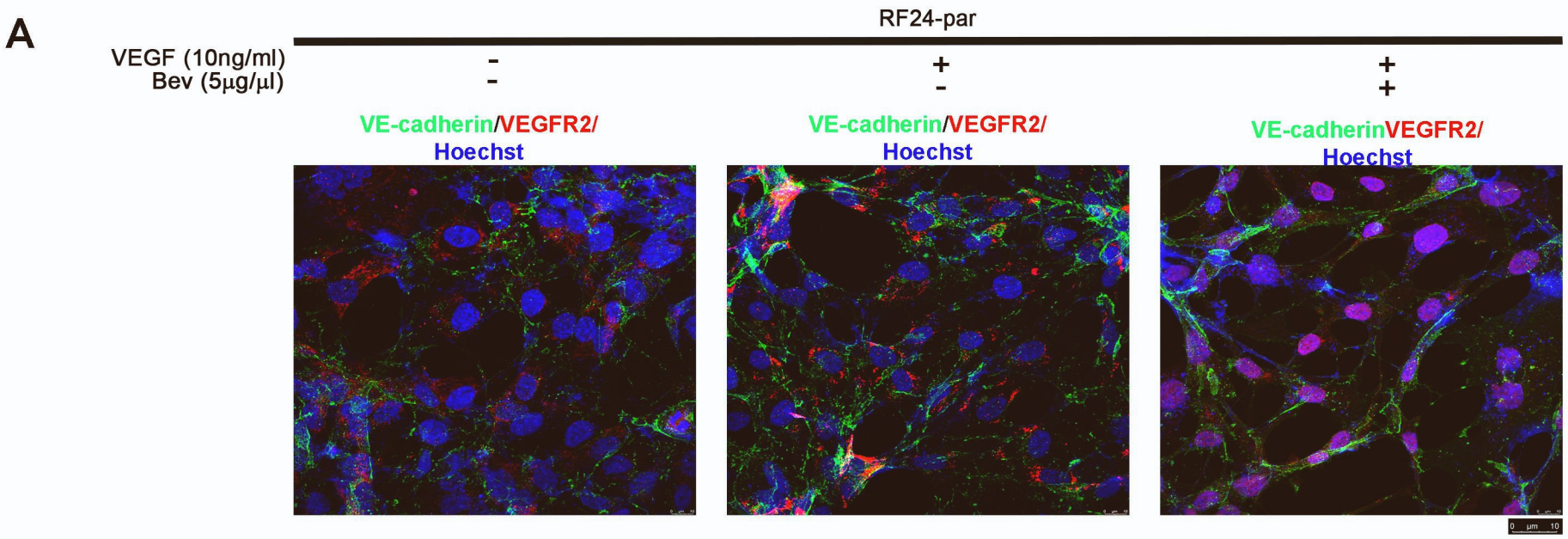

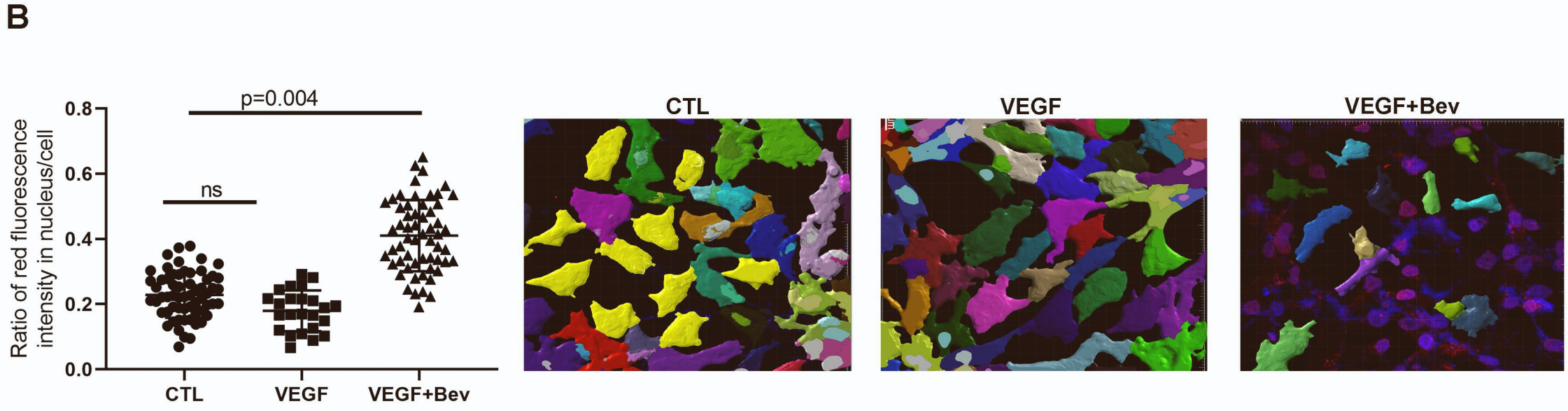

Supplemental Figure 6

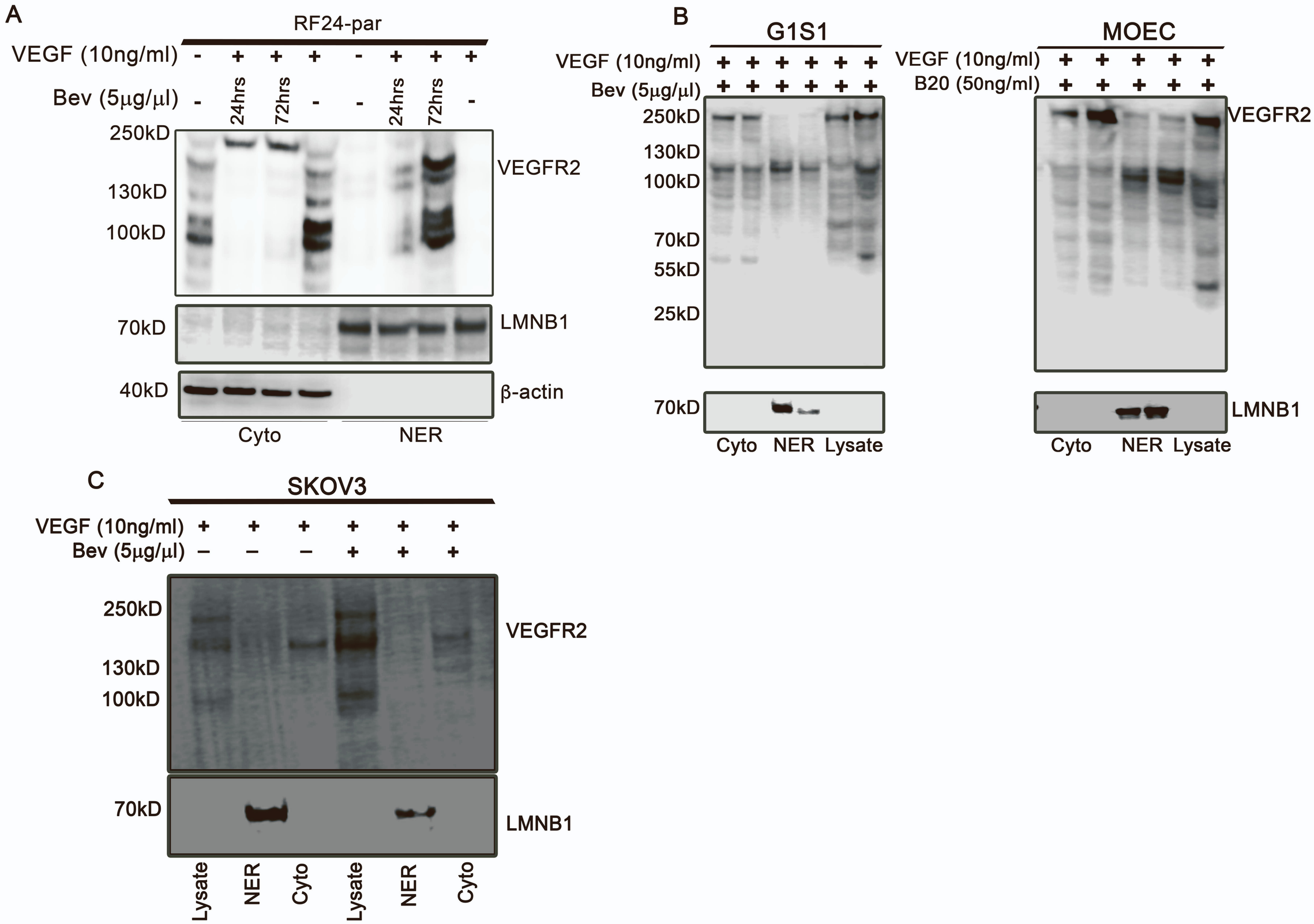

Supplemental Figure 7

A

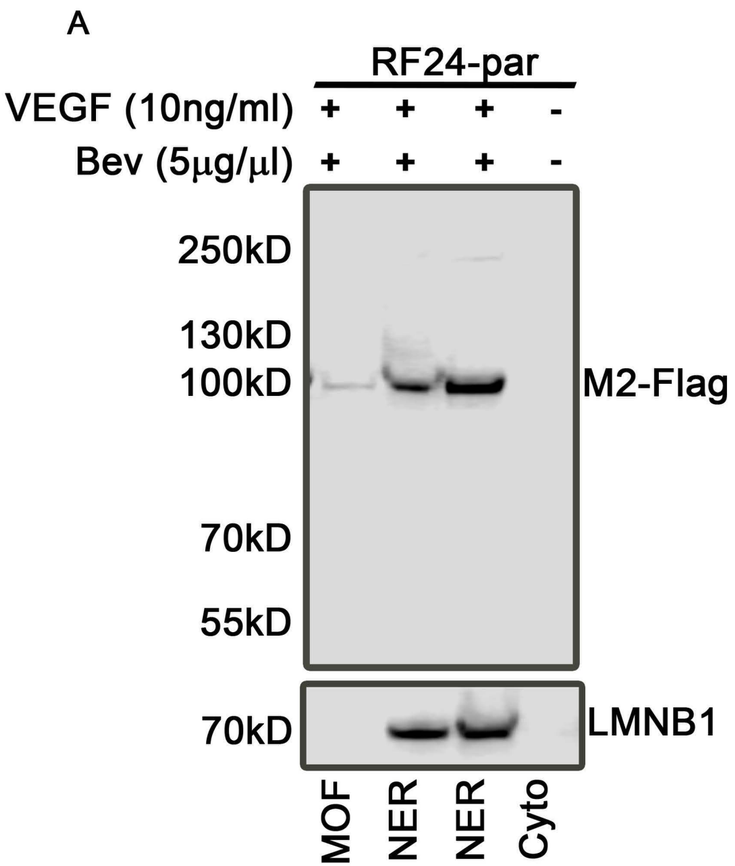

B

Uniprot	Protein Name	Gene Name	M.W. [kDa]	PEP
Q9C0C2	182 kDa tankyrase-1-binding protein	TNKS1BP1	181.79	4.55E-09
P47756	F-actin-capping protein subunit beta	CAPZB	31.35	7.84E-176
P0C0L5	Complement C4-B	C4B	192.80	1.90E-12
P13796	Plastin-2	LCP1	70.29	2.34E-13
O15231	Zinc finger protein 185	ZNF185	73.53	<1.0E-307
P19256	Lymphocyte function-associated antigen 3	CD58	28.15	5.88E-02

C

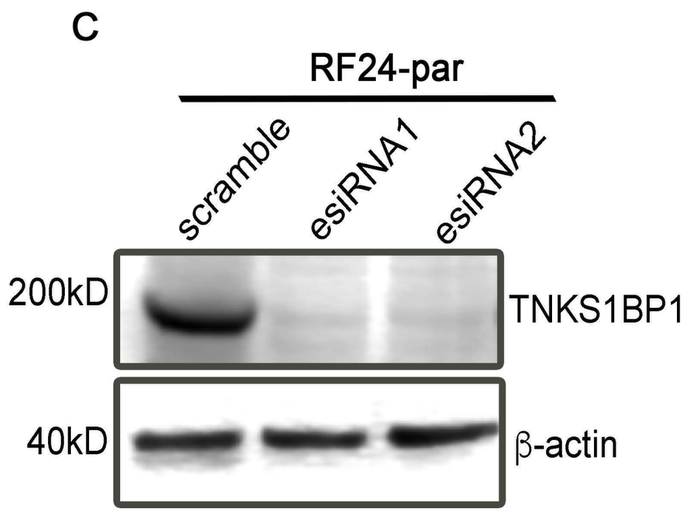

D

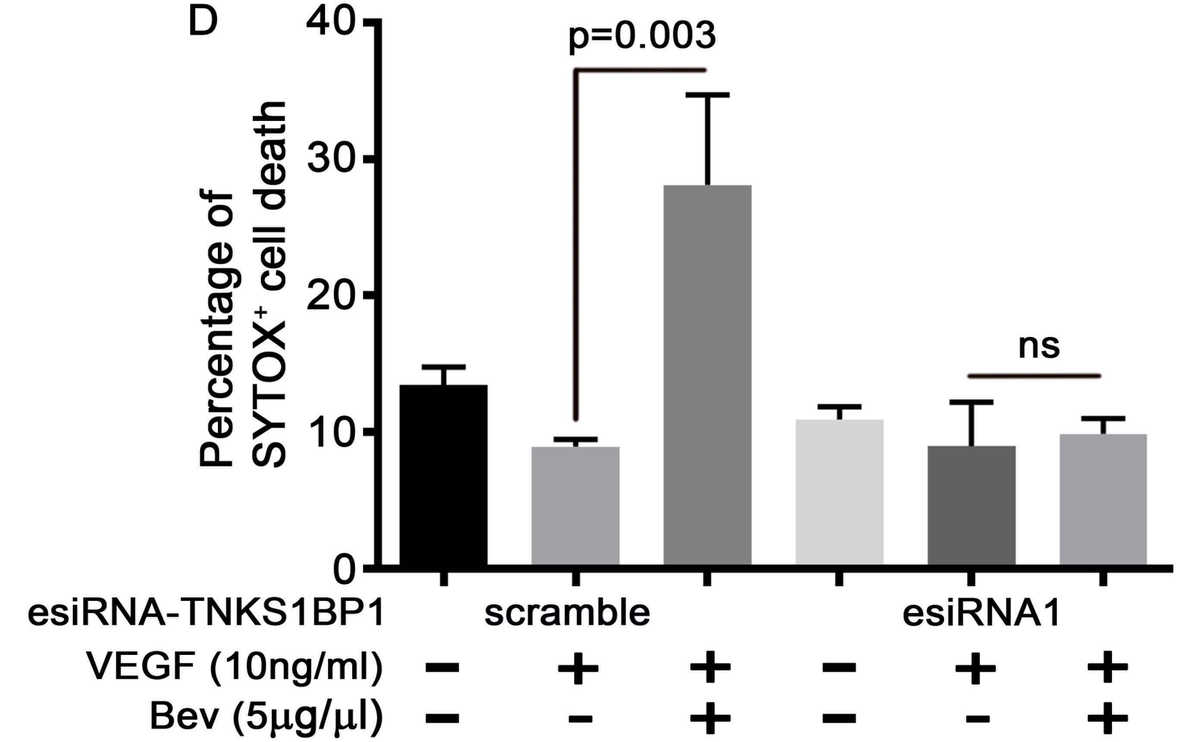

Supplemental Figure 8

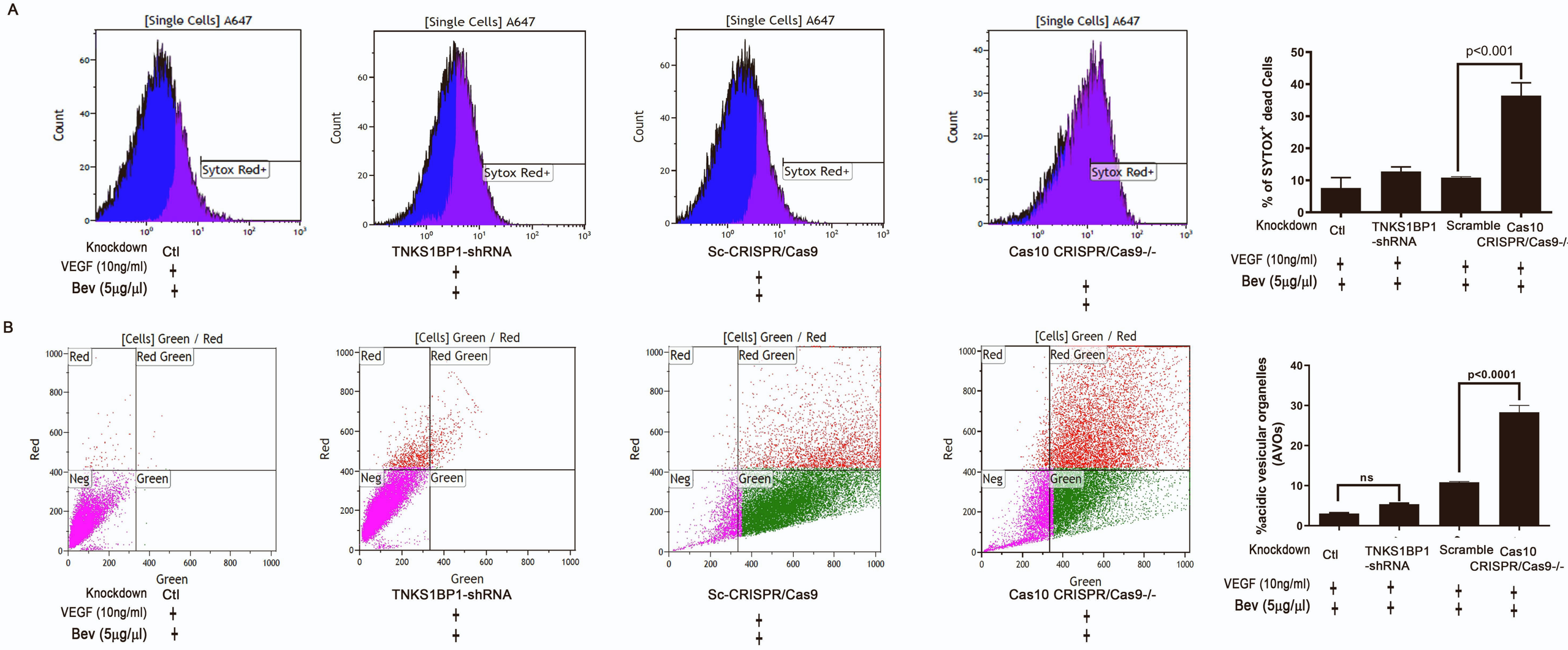

Supplemental Figure 9

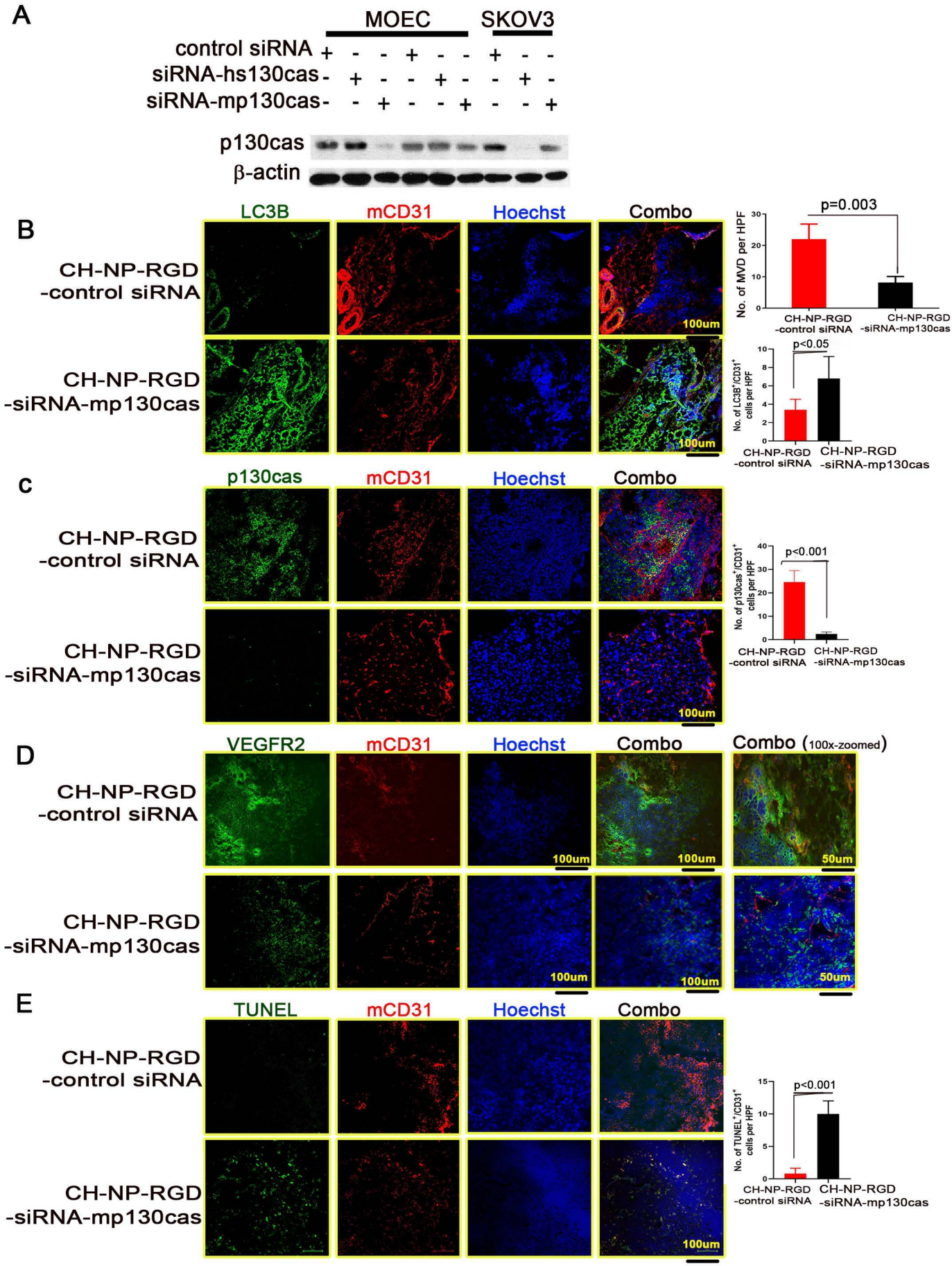

Supplemental Figure 10

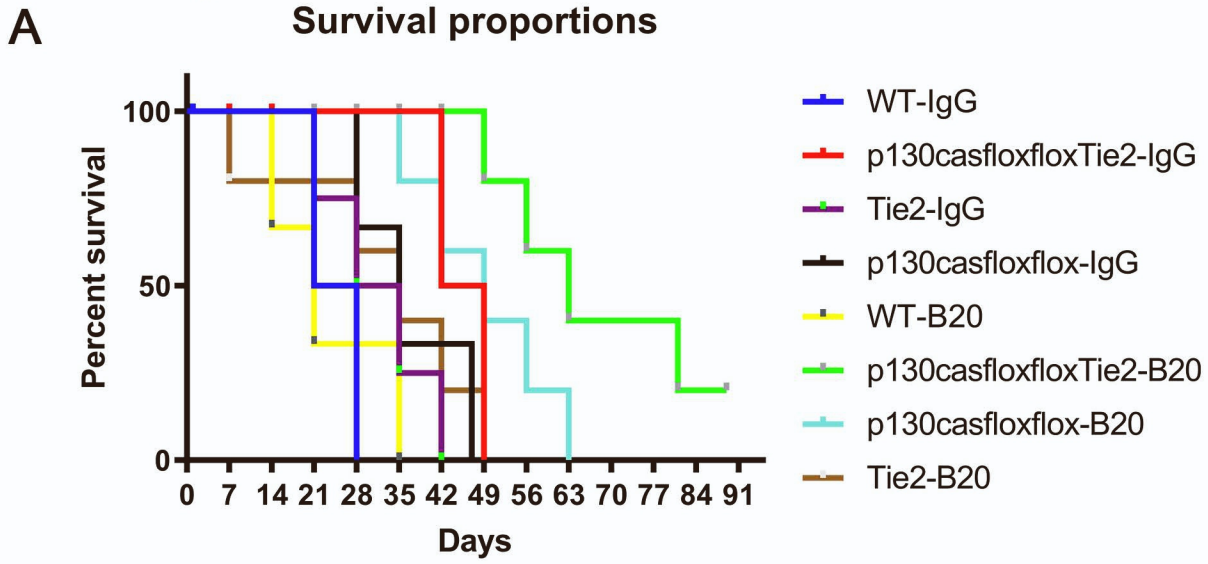

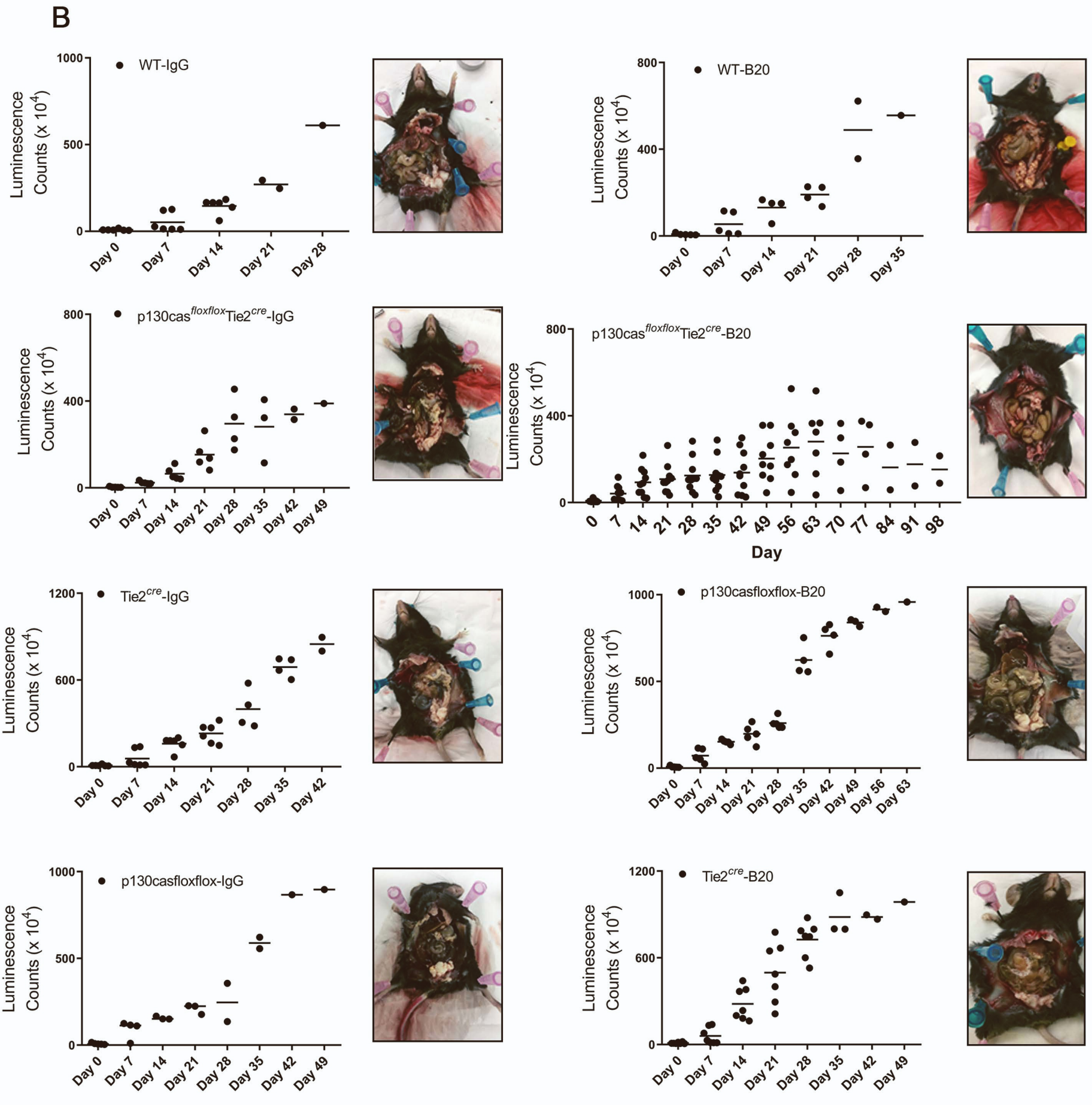

Supplemental Figure 11

A

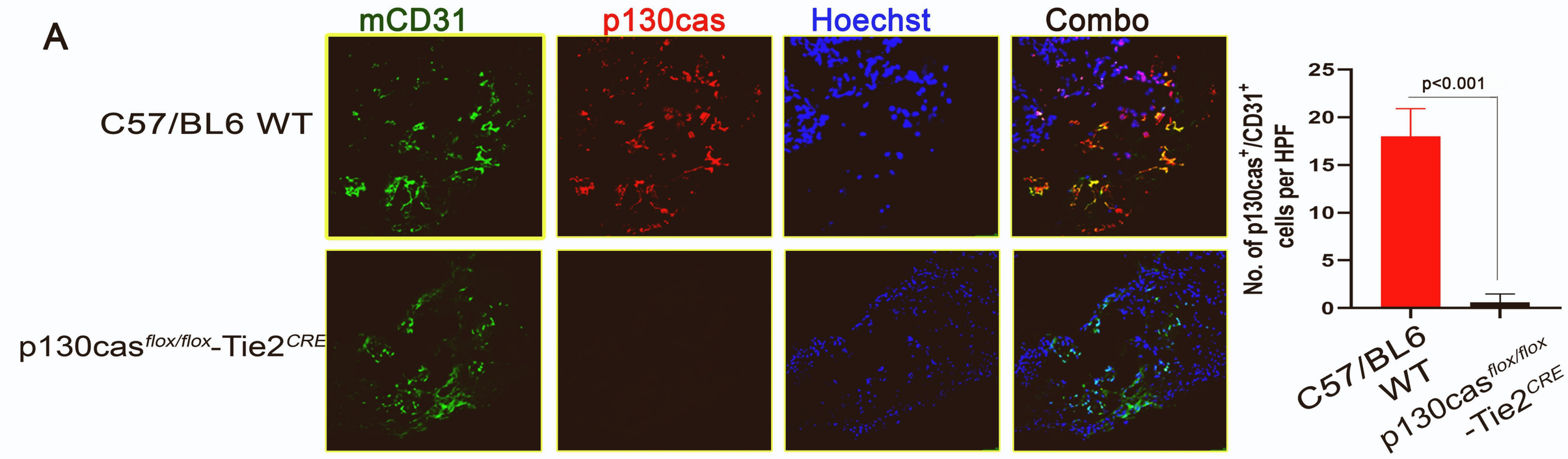

B

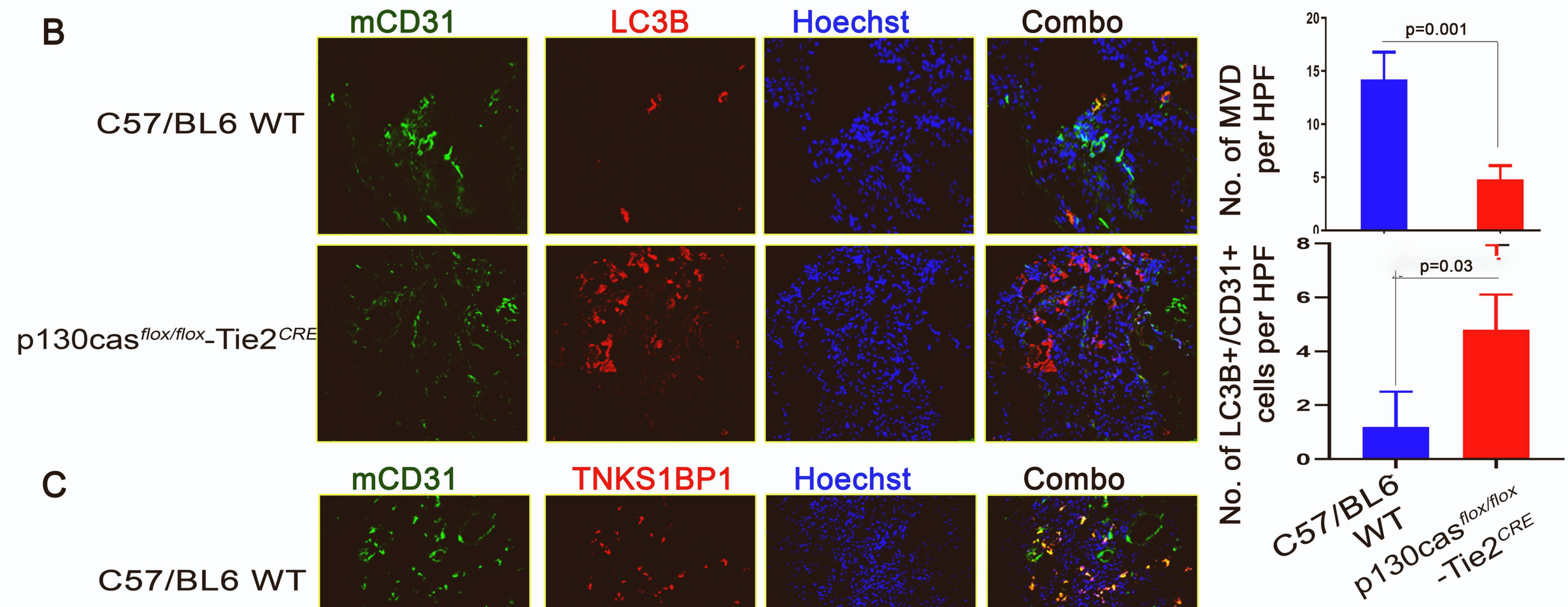

C

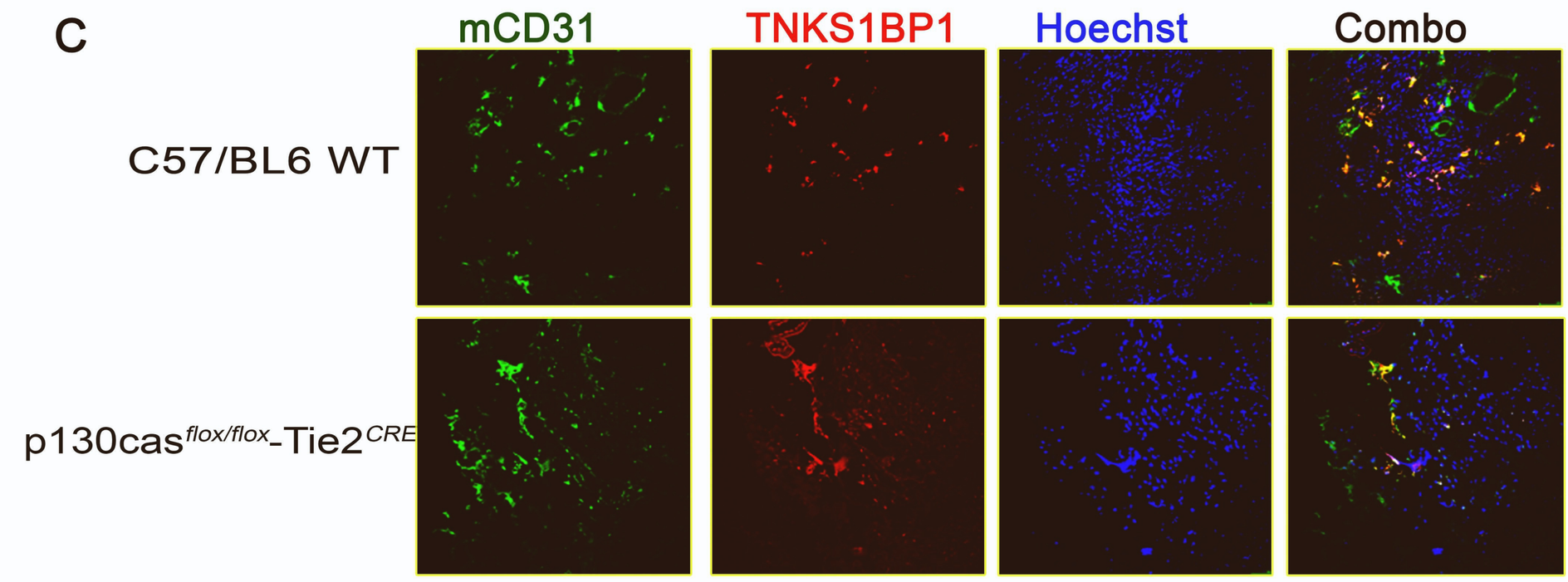

D